Computational Materials Science 190 (2021) 110312

Contents lists available at ScienceDirect

Computational Materials Science

journal homepage: www.elsevier.com/locate/commatsci

Microscopic mechanism of radionuclide Cs retention in Al containing C-S-H nanopores

Eduardo Duque-Redondo [a,*], Kazuo Yamada [b], Jorge S. Dolado [c], Hegoi Manzano [d]

[a] Department of Physical Chemistry, University of the Basque Country UPV/EHU, Aptdo. 664, 48080 Bilbao, Spain
[b] Fukushima Branch, National Institute for Environmental Studies, Miharu, Tamura, Fukushima 963-7700, Japan
[c] Centro de Física de Materiales, CFM-CSIC-UPV/EHU, Paseo Manuel de Lardizabal, 5, 20018 San Sebastián, Spain
[d] Department of Physics, University of the Basque Country UPV/EHU, Aptdo. 664, 48080 Bilbao, Spain

ARTICLE INFO

Keywords:
Calcium silicate hydrate
Calcium alumina silicate hydrate
Cement
Ion adsorption
Ion diffusion
Molecular dynamics

ABSTRACT

Cementitious materials act as a retaining barrier, immobilizing liquid and solid radioactive waste and preventing their release into the biosphere. The retention capability of hydrated cement paste and its main hydration product, C-S-H gel, has been extensively explored experimentally for many alkali and alkaline earth cations. Nevertheless, the retention mechanisms of these cations at the molecular scale are still unclear. In this paper, we have employed molecular dynamics simulations to study the capacity of C-S-H to retain Cs, Ca and Na, analyzing the number of high-affinity sites on the surface, the type of sorption for each cation and the diffusivity of these ions. We have also explored the impact of aluminum incorporation in C-S-H and the effect of the pore size. We have found strong competition for surface sorption sites, with notable differences in the retention of the cations under study and remarkable enhancement of the adsorption in C-A-S-H concerning C-S-H and greater diffusion of non-adsorbed species at larger pore sizes.

1. Introduction

Since the very beginning of the nuclear age, radioactive waste has been immobilized converting raw waste, with mobile contaminants, into a stable solid form or wasteform. These conditioning processes reduce the potential migration of those contaminants [1,2], including radionuclides and facilitate handling, transport, storage and disposal of radioactive wastes [3]. Different immobilization technologies, such as cementation, bituminization or vitrification, have demonstrated to be viable and have been widely applied for years [4–7].

Cementation has been used worldwide by the nuclear industry for immobilization of radioactive, hazardous and mixed waste since cementitious materials act as a diffusion barrier thanks to their large surface area which provides multiple sorption and reaction sites [8–11]. Moreover, these materials have many other advantages, such as the low-cost processing, high thermal, chemical and physical stability of the resulting wasteform, high durability, they are non-flammable and not degraded by radiation or the possibility of being processed remotely [12,13].

Ordinary Portland cement (OPC) is the most common cement-type used in radioactive waste worldwide [14] and calcium silicate hydrate (C-S-H) gel constitutes the main hydration product of OPC, representing about the 60–70% of the fully hydrated cement paste. Thus, the final properties of cement depend mainly on C-S-H gel.

Cementation has been used in order to retain ^{137}Cs, one of the most dangerous short-to-medium-lifetime fission products due to its high volatility and water solubility. Even though cement-based wasteforms have been proved to maintain radioactive species safely isolated from the environment for a long time, these species would eventually be released by leaching mechanisms [2]. Consequently, there is considerable interest in understanding and predicting the migration of the species located in the pores through the cement matrix. For that reason, there are many experimental studies reported on Cs immobilization/sorption in cement and concrete [14–16].

For concrete, conclusions are difficult to draw, since aggregates, variety of samples and differences in measurement techniques may have a huge impact on the Cs uptake. For cement and C-S-H, it has been found that Cs retention is enhanced at low pH, since at basic pH there is a considerable amount of calcium hydroxide that can saturate the surface adsorption points, reducing the binding capacity of Cs ions. In general, it is well recognized that Cs retention is better for low Ca/Si ratios and when a moderate amount of Al is present [16,17]. The retention can be also improved by the incorporation of some additives such as clays or zeolites [18,19]. However, it is also important to note that Cs will have

* Corresponding author.

https://doi.org/10.1016/j.commatsci.2021.110312
Received 16 July 2020; Received in revised form 12 January 2021; Accepted 13 January 2021
Available online 23 January 2021

to compete with other alkali ions, like Na and K, common in cement and C-S-H. The adsorption and retention mechanisms are considered to be by a cationic exchange between interlaminar Ca ions and Cs.

Notwithstanding these works, the immobilization mechanisms and the dynamics of the radioactive species are complex processes and are not fully explained experimentally. In this way, molecular dynamics (MD) simulations can be employed to gain insight into the adsorption and transport of Cs at atomic level. In this regard, many researchers have taken tobermorite mineral as a model system to study Cs retention in C-S-H, specially Komarneni, Roy and coworkers [20–27]. They found that tobermorite 14 Å has a considerably lower cation exchange capacity and selectivity towards Cs than tobermorite 11 Å. Essentially, in tobermorite 11 Å, the silicate chains merge across layers by Q^3 sites forming zeolite-like cavities with great cation exchange capability [25]. On the other hand, there are no Q^3 silicate species in tobermorite 14 Å and the exchange with interlaminar Ca ions is negligible, so Cs adsorption only takes place on surface defects [22]. These studies have also suggested that the presence of charge defects, form by aliovalent substitutions of Si^{4+} by Al^{3+}, enhances the adsorption [20]. C-S-H gel structure is, in general, more similar to that of tobermorite 14 Å [28–30].

In this work, molecular dynamics simulations are employed to study the interactions between Cs ions and the C-S-H surface, as well as the retention capability of C-S-H gel and the dynamics of Cs in 1 nm gel nanopores. The adsorption and transport of other common alkali and alkaline earth cations present in C-S-H gel, like Na or Ca, are also investigated. These cations are confined in the gel pore both individually and jointly with Cs ions to evaluate the effect of size and charge in the electrostatic sorption and the competition between these ions for the available sorption sites from the C-S-H surface. Furthermore, we have also studied the impact of the incorporation of aluminum in C-S-H to form C-A-S-H (calcium alumina silicate hydrate) and the effect of the nanopore size. On the one hand, the Al incorporation causes an increase of the net negative charge of the surface, which may enhance the binding capacity of the C-A-S-H surface to the cations mentioned before regarding the C-S-H surface [31]. On the other hand, the expansion of the pore space may result in a decrease of the nanoconfinement effect, facilitating the mobility of the confined water and, consequently, the release of the confined species by leaching mechanisms [32]. Atomistic simulations have been recently employed to study the adsorption of radionuclide cations, like ^{137}Cs, in C-S-H gel and related clay minerals, such as tobermorite and jennite [33–38]. However, to the best of our knowledge these studies do not explore the competitive adsorption of Cs in presence of other cations, neither the effect of the presence of Al on the C-S-H gel nor the impact of the pore size in transport and retention of Cs ions.

2. Atomistic model and simulation details

We have followed a procedure similar to that proposed by Kovačević et al.[39] to build a C-S-H model with a Ca/Si ratio of 1.1. This Ca/Si ratio was selected in order to obtain good retention, since the retention is enhanced at low Ca/Si ratios, according to the findings of Glasser and Hong [40,41]. Fig. 1 is a descriptive scheme of the procedure followed to build the C-S-H model.

First (see Fig. 1a), the crystalline structure of tobermorite 14 Å [42] is taken as a starting point due to its structural proximity to the C-S-H gel [43,44]. The unit cell is replicated to obtain a simulation box with dimensions 2.6 nm × 3.1 nm × 3.3 nm, corresponding to the x, y and z-axis Periodic boundary conditions are applied to approximate a large (infinite) system.

Second (see Fig. 1b), the chemistry is modified in several steps. All water molecules from the interlaminar space are removed. Then, to increase the Ca/Si ratio of tobermorite 14 Å (0.83[42]) to the target 1.1, some of the bridging silicate groups of the chains are randomly deleted and Ca ions are incorporated randomly in the interlayer space.

Third (see Fig. 1c), the appropriate amount of water molecules are rationally inserted in the interlaminar space using a geometry-based algorithm [45,46] to place them. For C-A-S-H systems, we replaced 65% of the remaining bridging silicon by bridging aluminium [47,48], reaching an Al/Si ratio of 0.15 and Ca/(Si + Al) of 1.1. The isomorphic substitution of Si^{4+} by Al^{3+} originates a net negative charge. In order to maintain the electroneutrality of the system without modifying the amount of confined cations, some hydroxyl groups from the interlaminar space were removed. Once the chemistry matches the target, we run energy minimization and MD simulations to equilibrate the system. These simulations are done using the reactive force field ReaxFF [49], whose parameters are based on Si–O–H [50] set and extended for aluminosilicates with Al–O–H [51] and Ca–O–H [52] parameters. This force field allows the relaxation of the structure, volume and chemical reactions. Regarding the latter, the only chemical reaction observed is the dissociation of certain water molecules to form hydroxyl groups in some of the dangling oxygen atoms from the new Q^1 sites of the silicate chains created by the silicate deletion. The samples were relaxed in the isobaric-isothermal ensemble (NPT) for 5 ns at 300 K.

Finally (see Fig. 1d), after the relaxation with ReaxFF, we created gel pores from 1 to 5 nm expanding the interlaminar space. We have decided to study retention and diffusivity in gel pores, defined by Pinson et al. as all pores with widths between 1 and 10 nm [53], because below 1 nm, the electrostatic confinement of the species located in the interlaminar space is so high that their mobility of the confined species is very constrained, while at pores with width above 1 nm the confined water can flow, leading to leaching processes that may result in the release of the contaminants. Larger pores, such as capillary pores and macropores, have not been analyzed since they remain empty under high relative humidity and are usually considered to be devoid of bulk water and they only present a thin adsorbed layer of water on the walls [53]. Thus, leaching is more likely to occur in pores fully saturated with water, as gel pores. The created pores are filled with the necessary amount of water

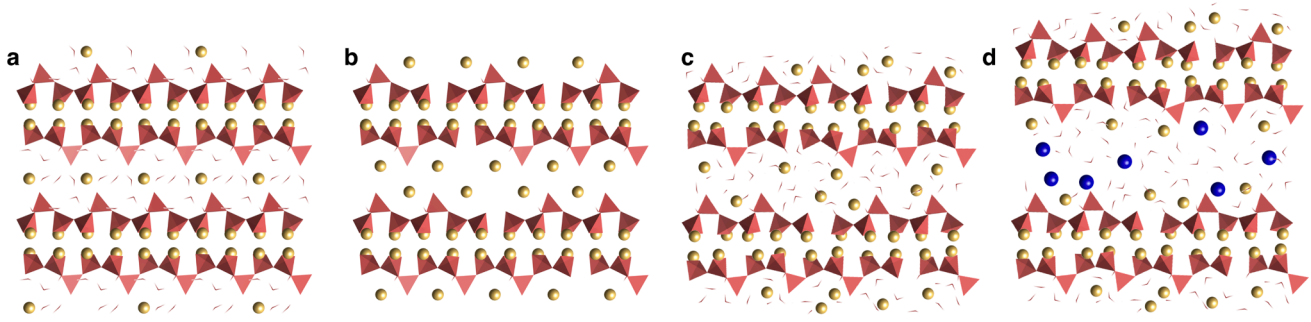

Fig. 1. Schematic procedure summarizing the main four steps for the development of the C-S-H gel structure drawn from tobermorite 14 Å as a starting point. The garnet tetrahedrons correspond to the silicates, water and hydroxyl groups molecules are illustrated as double and single red sticks and the yellow and blue balls represent the intrinsic Ca and the ions under study.

molecules to reach a density of 1 g/cm^3 and, at this point, the alkali and alkaline earth cations under study are incorporated into the pores, counterbalanced with hydroxyl groups. In this study, we have first analyzed the retention and diffusion of Cs, Ca and Na separately, for which we have built C-S-H and C-A-S-H models in whose pore spaces only one type of these cations is added, and then, we have studied the competition for the high affinity sites and its effect on diffusion by developing a C-S-H and a C-A-S-H models in which Cs, Ca and Na coexist in the interlaminar space. The concentration of these cations has been chosen attending to the work of Miyake et al.[24], who found experimentally that the maximum Cs/Ca ratio for tobermorite 14 Å was 0.85, considering only the exchangeable Ca ions. Therefore, we added to the pore space the appropriate amount of CsOH, NaOH and $Ca(OH)_2$ to achieve a 0.85 cation/Ca ratio in our C-(A-)S-H systems, equivalent to 1.62 cations per nm^2 of C-(A-)S-H surface. Since we have introduced extra Ca to the C-(A-)S-H systems, we will distinguish between the extra added Ca and the structural Ca in the C-(A)-S-H calling the latter "intrinsic Ca".

The C-(A-)S-H models are equilibrated, but instead of using ReaxFF, we have employed a combination of non-reactive force fields since ReaxFF has not been parameterized for Cs. More precisely, we have used CSHFF force field [54] (for the substrate), ClayFF [55] (for the aluminum in C-A-S-H) and the Åqvist [56] parameters (for the exchangeable ions).

All the molecular dynamics were carried out using LAMMPS [57]. The long-range Coulombic interactions were computed with the Ewald summation method [58] and the motion equations were integrated using the Verlet algorithm [59]. Initially, we carried out molecular dynamics in the canonical (NVT) ensemble for 0.5 ns at 300 K with a time step as large as 0.5 fs and a thermostat coupling constant of 0.1 ps. To equilibrate the atomic positions and volume under room conditions, the systems were further relaxed in isobaric-isothermal (NPT) ensemble for another 0.5 ns at 300 K and 1 atm with a barostat coupling constant of 1 ps. Finally, a canonical ensemble (NVT) simulation was performed for 0.1 μs at 300 K, to ensure that the diffusion is captured and other macroscopic observables have been relaxed and converge.

3. Results and discussion

3.1. Bulk structure validation

The final properties of the bulk C-(A-)S-H model are in agreement with experimental and molecular models reported by other authors, as can be seen in Table 1. Experimentally, the addition of Al in the synthesis of C-A-S-H may modify the structure of C-S-H, inducing a rise of the mean chain length (MCL). However, in our simulations, we have only substituted bridging Si atoms by Al to study the effect of the presence of a moderate amount of Al in the structure of C-S-H. Therefore, the MCL, as well as other parameters analyzed in Table 1, are not altered by the Al incorporation.

The substitution of the 65% of bridging silicon by aluminum to develop C-A-S-H results in the increase of the surface charge regarding C-S-H. This leads to an increase in the electrostatic interactions, which has an impact on the basal distances of these systems. Thus, it has been observed a slight decrease in the basal distance of C-A-S-H regarding the C-S-H ones for all the studied systems. The structural parameters of the C-(A-)S-H models are given in Table 2.

Table 1
Final properties for the bulk C-S-H model obtained from our simulations and the literature.

	C-S-H model	Literature
Ca/Si	1.1	1.1
MCL	5.67	5.9–6.6[60,61]
Ca-OH/Ca	0.23	0.08–0.20[61–64]
Si-OH/Si	0.32	0.35–0.38[62,63]

3.2. Pore density profiles

Once the bulk structure has been validated, we have analyzed the atomic distribution in the C-(A-)S-H systems by computing the density profiles of the species located in the nanopore. These profiles provide quantitative information about the arrangement of the species with respect to the C-(A-)S-H surfaces. Fig. 2 shows the density profiles of the species located in the interlaminar space of the three C-S-H and three C-A-S-H models in which only Cs, Ca and Na were introduced, respectively, along with a snapshot of the MD simulation corresponding to the analyzed interlaminar space for better comprehension. In order to build those density profiles, the positions of the atoms were recorded during 20 ns of simulation, then averaged and normalized.

For the analysis of the density profiles, the systems are divided into three parts following the Guggenheim interface convention [65]: the bulk solid, the liquid phase and the extended interfacial region between them in which water penetrates into the solid. In Fig. 2, only the interphase (z less than 0 Å) and the bulk liquid region (z greater than 0 Å) are represented. It must be noted that we have assigned to the interfacial limit between those regions the value 0 Å to facilitate the discussion. It can be seen that there are strong peaks for the analyzed cations just above and below the interfacial limit, which can be related to outer- and inner-sphere complexes. Additionally, there can be non-adsorbed species, hereafter called pore species, which are located in the liquid phase far from the C-(A-)S-H. These pore species are solvated by water molecules and, unlike inner- and outer-sphere complexes, do not interact with the C-(A-)S-H surface. The formation of inner- and outer-sphere complexes has already been reported for different ions confined in C-S-H [34,36,66,67]. Those works point out that the cations in inner-sphere configurations are partially dehydrated regarding pore species, completing their coordination shells by direct coordination to the C-S-H surface. In outer-sphere configurations, the cations are fully hydrated, with a solvation shell similar to that of dissolved (pore) ions that interacts with the C-S-H surface. Thus, the peaks of outer-sphere complexes are located farther from the surface than those of inner-sphere complexes, explaining the presence of strong peaks at shorter and farther distances from the surface for all the analyzed cations. However, there are significant differences in the distribution of each cation (Cs, Ca, Na) throughout the pore.

The comparison of the density profiles of the systems which contain the different cations under study allows the evaluation of the effect of cationic size and charge in their approach to the C-(A-)S-H surfaces, as well as the impact of aluminum incorporation comparing C-S-H and C-A-S-H. It should be noted that all the studied ions tend to be mainly located close to the surfaces, as a consequence of the electrostatic interactions between the cation (positively charged) and the surface (negatively charged). In clays, for instance, the charge is more diffuse in comparison with C-(A-)S-H, since charge defects in clays are distributed homogeneously and they are frequently located in inner layers, while the C-(A-)S-H systems have specific structural defects in the surface. Thus, in clays, some ions prefer to be completely hydrated in the center of the pore rather than adsorbed on the surface depending on the water content and clay type [68].

It should be noted that the increase of the negative charge of the surface by the isomorphic substitution of Si^{4+} by Al^{3+} in C-A-S-H results in better retention of the cations since the number of pore ions (non-

Table 2
Basal distances for the C-S-H systems and their C-A-S-H analogous.

d_{001} (Å)	C-S-H	C-A-S-H
Cs	13.88	13.48
Ca	13.18	12.92
Na	13.06	12.24

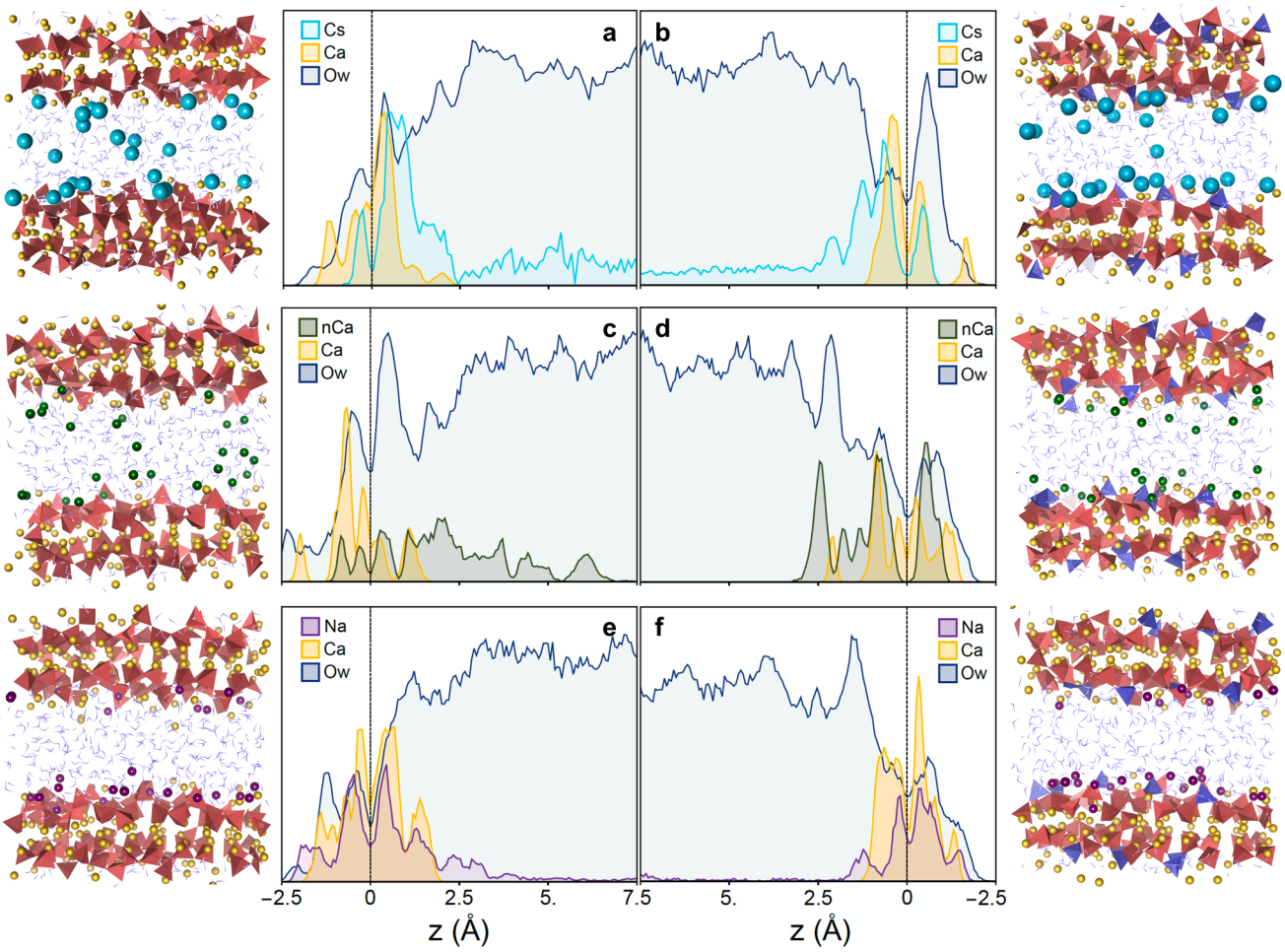

Fig. 2. Density profiles and their corresponding snapshots of the MD simulation for C-S-H (left) and C-A-S-H (right) systems which incorporate only Cs (a, b), Ca (c, d) and Na (e,f) at concentrations of 1.62 cations per nm^2 of C-(A-)S-H surface. The black dashed line corresponds to the upper interface boundary. Cs, Ca and Na are represented as light blue, green and purple balls, respectively, whereas the intrinsic Ca are the yellow ones; the garnet and blue tetrahedrons correspond to the silicate and aluminum chains and the water molecules and hydroxyl groups are illustrated as blue sticks.

adsorbed) drops significantly in C-A-S-H. However, there are big differences between the cations under study. On the one hand, there are more Cs ions in the center of the pore than of any other cation, suggesting that the adsorption energy of Cs is lower than its hydration energy. On the other hand, Na cations are totally adsorbed on the surface, both in C-S-H and C-A-S-H, while Ca is partially desorbed in C-S-H but not in C-A-S-H. The lower Ca uptake may be due to higher repulsive electrostatic forces between Ca ions (divalent cation) and other cations previously adsorbed in the surface, but also to a higher coordination shell that could make more difficult its approach to the surface. The coordination shell of Cs, Ca and Na is analyzed and described in detail in the Supplementary Information. Finally, it should be noted that the intrinsic Ca atoms are located close to C-(A-)S-H surface, forming either inner- or outer-sphere complexes. The added alkali and alkaline earth cations are not able to displace the intrinsic Ca from their surface adsorption sites since there is no intrinsic Ca desorbed in the nanopore. This suggests that the intrinsic Ca may have higher adsorption energies than the added cations.

3.3. Adsorption configuration

We have seen that the cations incorporated in C-(A-)S-H nanopores can be accommodated in different settings, being classified into three adsorption configurations: inner-sphere, outer-sphere and pore cations. It is necessary to evaluate how the cations under study are adsorbed to characterize their behaviors. Table 3 shows the relative amount of the considered cations in each sorption configuration. It must be noted that we have added an identical number of cations (1.62 cations per nm^2 of C-(A-)S-H surface) in each system to compare them. Thus, Table 3 shows that there are more non-adsorbed (pore) Cs than Ca and much more than pore Na. The higher number of non-adsorbed Cs ions may be attributed to the moderate charge (monovalent cation), the higher atomic radius of Cs ions and the larger coordination shell regarding Ca and Na (see Coordination Shell Section from Supplementary Information), which may hinder their approach to these cations to the C-(A-)S-H surface and its adsorption. On the other hand, Na is strongly adsorbed, exhibiting the highest percentage of ions in inner-sphere sites and the lowest relative amount of ions in the pore configuration. Ca ions present better adsorption rates than Cs, but not as good as the Na despite having a similar atomic radius. This is probably due to the electrostatic repulsion

Table 3
Percentage of ions adsorbed by inner-sphere/outer-sphere/pore configurations for the studied cations in C-S-H (left) and C-A-S-H (right). The total number of cations, 100%, is equivalent to 1.62 cations per nm^2 of C-(A-)S-H surface.

	C-S-H			C-A-S-H		
Cation	Inner	Outer	Pore	Inner	Outer	Pore
Cs	16%	49%	35%	32%	41%	27%
Ca	22%	59%	19%	35%	52%	13%
Na	52%	40%	8%	54%	42%	4%

between the added Ca ions and the intrinsic Ca of the C-(A-)S-H surfaces due to the charge divalent of Ca compared to the monovalent of Na ions. The adsorption configurations of the intrinsic Ca for all the analyzed systems are given in Supplementary Table 3.

Regarding the aluminum incorporation, it can be seen that the retention is better in C-A-S-H than in C-S-H, since a significant decrease of the cations dissolved in the pore is observed in presence of aluminum. Indeed, the amount of inner-sphere complexes for Ca and Cs ions rises about 50% and 40% respectively in C-A-S-H, while the amount of non-adsorbed species decreases up to 40%. The retention of Na in C-A-S-H is also enhanced despite its retention is C-S-H was already very good. In any case, the same trend in retention is observed in both C-S-H and C-A-S-H: Na > Ca > Cs.

The data from Table 3 can be expressed as the number of available sorption sites per area of C-(A-)S-H surface (Table 4). These values are consistent with the amount of adsorbed cations on the surface. The increase of the negative charge of the surface in C-A-S-H provokes a notable rise of the inner sorption sites and a slight decrease in the outer adsorption. However, the global number of sorption sites is higher in C-A-S-H than in C-S-H. Na has the highest number of sorption sites, but the incorporation of aluminum increases markedly the number of sorption sites for Cs and Ca.

3.4. Adsorption enthalpies of cations

We have computed the adsorption enthalpy, ΔH_{ads}, of the studied species using the following expression:

$$\Delta H_{ads} = \Delta H_{C(A)SH/Cs} - \Delta H_{C(A)SH} - \Delta H_{M/H2O}$$

where $\Delta H_{C(A)SH/M}$ is the enthalpy of the system under study, $\Delta H_{C(A)SH}$ the enthalpy of the C-S-H substrate without the cation under study and $\Delta H_{M/H2O}$ is the enthalpy corresponding to the respective cation in bulk water. According to this definition, the more negative the enthalpy, the more favorable the adsorption of the cation.

The values of the adsorption enthalpies for the cations under study are given in Table 5. The trend obtained for the adsorption enthalpies is $\Delta H_{Ca} < \Delta H_{Na} < \Delta H_{Cs}$ both in C-S-H and C-A-S-H. It can be seen that the adsorption of Ca ions is the most favorable, followed by Na adsorption. The adsorption of Cs is favorable, but not as much as for the other two studied cations. This is in good agreement with the observed retention since Ca and Na, with the most favorable adsorption enthalpies, are the best-retained cations, whereas Cs is the least retained since its adsorption is the least favorable. It is also remarkable that the adsorption in C-A-S-H is more favorable due to the higher charge defects in the C-A-S-H.

Comparing the values from Table 5 with the average adsorption enthalpy measured for intrinsic Ca, −6.73 kcal/mol, we can also explain why the studied cations are not able to desorb the intrinsic Ca from C-(A-)S-H surfaces.

3.5. Diffusion coefficients

Together with good retention, it is also equally important to low diffusion coefficients of the confined species to avoid leaching processes, which can lead to the release of the contaminants into the environment. To measure the diffusion coefficients of the cations under study, we have employed molecular dynamics to obtain the mean square displacement

Table 4
Number of inner/outer adsorption sites per nm^2 of C-(A-)S-H and the sum of them for the systems that incorporate Cs, Ca and Na.

Sorption sites/nm^2	C-S-H Inner	Outer	Sum	C-A-S-H Inner	Outer	Sum
Cs	0.3	0.8	**1.1**	0.6	0.7	**1.3**
Ca	0.4	1.0	**1.4**	0.6	0.9	**1.5**
Na	0.9	0.7	**1.6**	0.9	0.7	**1.6**

Table 5
Adsorption enthalpies for the studied cations in C-S-H (above) and C-A-S-H (below).

	Cs	Ca	Na
ΔH_{CSH} (kcal/mol)	−0.20	−6.51	−5.35
ΔH_{CASH} (kcal/mol)	−0.64	−6.79	−5.63

(MSD). The MSD measures the deviation of the position of a particle with respect to a reference position over time and is defined by the following equation [69]:

$$MSD = \langle |r(t) - r(0)|^2 \rangle$$

Einstein [70] related the MSD with the self-diffusion coefficient (D) through the following expression:

$$D = \frac{1}{2d} \lim_{t \to \infty} \frac{MSD}{t}$$

being d the dimensionality of the system. Therefore, the diffusion coefficient can be computed from the linear fit of the MSD plot as a function of time. In this work, the diffusion coefficient for a given cation/molecule is computed from the average of the individual diffusion coefficients of each cation/molecule in the system of a given species.

The average diffusion coefficients obtained through the MSD for Cs, Ca and Na in C-S-H and C-A-S-H are given in Fig. 3. It can be clearly seen that Cs ions have by far the highest diffusion coefficients. Na ions exhibit diffusion rates one order of magnitude lower than Cs, but one order of magnitude higher than Ca ions. These results are in agreement with the adsorption enthalpies obtained for those cations and with the tendency of intrinsic diffusivity of these cations in bulk water (see Table 6). Thus, even in absence of C-(A-)S-H surfaces, Cs cations present a higher diffusion than Na and Ca, showing the same trend in bulk water and confined in C-(A-)S-H nanopores.

The fact that Ca ions have diffusion coefficients one order of magnitude lower than Na may seem contradictory with our previous findings since we have seen that the Na is more adsorbed and penetrates deeper in C-(A-)S-H surface than Ca ions. However, the charge density of alkali ions is much lower than the one alkaline earth ions: Ca and Na have a similar radius (see Table 6), but the charge density of Ca, a divalent cation, is much higher than the one in Na, a monovalent cation. Thus, the electrostatic interactions established by Na ions are expected to be weaker than in Ca, resulting in higher diffusivity.

It should be noted that the average diffusion coefficient for water in C-(A-)S-H nanopores is one order of magnitude lower than the values reported for bulk water due to the well-known effect of nanoconfinement [75–78]. The experimental [79] and simulated [80] (using the SPC/E water model) values for the diffusion of bulk water are ~2.3 10^{-9} m^2s^{-1} and ~ 2.5 10^{-9} m^2s^{-1}, respectively, while the average diffusivity

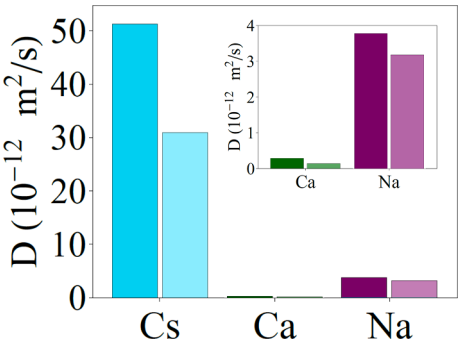

Fig. 3. Average diffusion coefficients for Cs (in blue), Ca (in green) and Na (in purple) in C-S-H (dark colors) and C-A-S-H (light colors). The inset was included for better visualization of the coefficients of Ca and Na ions.

Table 6
Atomic and ionic radius and diffusion coefficient of Cs, Ca and Na in bulk water.

	Atomic radius [71] (pm)	Ionic radius [72] (pm)	Diffusion in bulk water [73,74] ($m^2\ s^{-1}$)
Cs	260	181 (+1)	$20.7\ 10^{-10}$
Ca	180	114 (+2)	$7.9\ 10^{-10}$
Na	180	116 (+1)	$13.3\ 10^{-10}$

of water molecules in our nanopores is $\sim 2.6\ 10^{-10}\ m^2s^{-1}$. This fact, combined with the interactions with the negatively charged silanol groups on silicate chains provokes a drastic reduction of the diffusivity of the cations regarding bulk water. Moreover, we can compare our values with those reported for cations confined on clays. Na and Ca cations located in interlaminar spaces of common clays, such as montmorillonite or vermiculite, exhibit diffusion coefficients about $1\text{-}6{\cdot}10^{-10}$ m^2/s [81–83] and $7\text{–}10{\cdot}10^{-10}$ m^2/s [83,84] respectively. These values are two orders of magnitude higher than the values obtained in C-(A-)S-H, which may be caused by the higher charge in C-(A-)S-H surface with respect to the ones of clays. Contrary to C-(A-)S-H, in clays, the diffusivity of Cs is lower than the diffusion of Ca and Na, exhibiting diffusion coefficients between $1{\cdot}10^{-10}$ m^2/s [81,85] in the case of montmorillonite and $8{\cdot}10^{-12}\ m^2/s$ [86,87] in bentonite. This is due to the tendency of Na and Ca cations to stay in the middle of the interlayer spaces in clays [82,88], being surrounded by water molecules, whereas Cs ions tend to remain close to the clay surfaces [81]. Therefore, the Cs diffusion coefficients for C-S-H are in the low range of coefficients found for Cs in clays.

Fig. 3 also shows a comparison between the diffusion coefficients of the cations in C-S-H and C-A-S-H. The increase of the net negative charge on the surface of C-A-S-H results in an enhanced retention capacity, reducing the diffusion of all the cations. In that sense, the incorporation of aluminum has a huge impact on the diffusivity of Cs, decreasing its coefficient by about 40% in comparison with the one in C-S-H. The retention of Na in C-S-H was remarkably good, so the impact of Al incorporation on Na is more restricted, with a reduction of 16% in its coefficient. The sharp reduction of the diffusion coefficients in C-A-S-H is related to changes in the amounts of each type of cation induced by the aluminum incorporation. These changes provoke an increasing number of ions adsorbed in inner and outer-sphere sites due to the increase of the electrostatic interactions and there is, consequently, a decrease in the number of ions in the pore.

We have also determined the diffusivity of the cations under study in the different sorption configurations (see Supplementary Fig. 4), finding that the coefficients of the pore cations are up to two orders of magnitude higher than for the adsorbed cations in inner- and outer-sphere sorption configurations for the three cations since the motion of the adsorbed cations is restricted due to their interaction with the C-(A-)S-H surfaces.

3.6. Residence time

Along the simulation time, the cations form and break bonds continuously with the different oxygen atoms. We have characterized the overall diffusion and the diffusion while the cations are adsorbed in specific sites. However, for a complete picture, we need to evaluate how long the cations remain in those sites. For that purpose, we have computed the autocorrelation function (ACF) to define quantitatively the strength of those bonds between the cations and the oxygen atoms through their residence lifetimes. This function gives the probability of fulfilling certain criteria, such as the existence of a chemical bond, without interruption at a given time τ, being those criteria fulfilled at the initial time 0. The autocorrelation function is described by the following equation [69]:

$$ACF(\tau) = N\langle\sum_{t=0}^{T-\tau}\beta_{ij}(t+\tau)\hat{A}\cdot\beta_{ij}(t)\rangle_{i,j}$$

being β_{ij} the autocorrelation of a simple function for a given pair of particle i,j, and its value is 1 as long as the criteria are fulfilled and switches to 0 as soon as the criteria fail for the first time. In other words, ACF is 1 when the M−O pair is bonded but immediately takes the value 0 when the bond is broken. It is worth pointing out that the shown ACF is the average of all the M−O pairs in our simulations, so the more frequent the bond breakage, the faster the ACF reaches the value 0. Thus, it is possible to quantify the strength of those bonds by comparing the deviation of ACF from the initial value 1.

Fig. 4 shows the autocorrelation functions for M−O pairs. It can be seen that the longest relaxation time corresponds to metal-surface oxygen bonds, followed by metal-hydroxyl groups, while the bonds between cations and water molecules have the shortest relaxation time. This indicates that the interactions between the cations under study and oxygen from the surface are the most stable, with half-time substantially higher than the bonds with the other oxygen types. The higher stability of the interactions between the cation and hydroxyl groups with respect to water molecules is attributed to stronger electrostatic interactions with the hydroxyl groups, especially intense in Ca, due to its divalent charge. From this graph, it can also be drawn a stability trend according to the cation type: Ca-O bonds are stronger than Na-O, being Cs-O the weakest ones. The highest residence time in high-affinity sites corresponds to Ca atoms, whose half-life time for Ca-Os bonds is about 9.3 ns, followed by Na with a half-life time of 3.0 ns. Cs atoms exhibit the shortest residence time, with Cs-Os half-life times of 0.4 ns. This trend is the same that the one found for the diffusion coefficients of these cations. Thus, those atoms, which are capable of establishing stronger M−Os interactions, are more retained by the surface, leading to lower diffusion coefficients. The longer residence times of Ca can also explain why these atoms have the lowest diffusion coefficients, despite being coordinated to less the oxygen atoms from the surface than any other cation.

3.7. Direct competition

So far, we have studied the adsorption of the cations separately, but, commonly, they appear together in cement and concrete. In order to study the direct competition between these cations by the high-affinity sites in C-S-H and C-A-S-H, we have developed C-(A-)S-H systems in which, Cs and Na are incorporated in the nanopores with a total Cs + Na concentration of 1.62 cations per nm^2 of C-(A-)S-H surface. To introduce these cations, we have employed the swap Monte Carlo method. This technique enables the exchange of a given cation type with an imaginary ideal reservoir of another given cation type, (Cs and Na in this work) and can be applied following two approaches. In the first approach, the probabilities of having an atom swap are determined by the temperature of the simulation and the chemical potential of the swapped species, following the Metropolis criterion to decide whether the atom swap attempt is accepted or not. It should be noted that the kinetic energy of the swapped cations does not change before and after the swap because their velocities are scaled by the ratio of their masses. Therefore, following this approach, the initial composition of our systems may change since the Cs-Na fraction is governed by the difference in the chemical potentials of Na and Cs. Indeed, at room conditions, this difference is large enough to lead to C-(A-)S-H system in which all Cs ions are replaced by Na. Hence, to study *in situ* competition of Cs and Na in C-A-S-H nanopores, we have followed the second approach in this study, in which the Cs-Na fraction is preserved because the only kind of swap allowed is the exchange of one atom type (Cs or Na) by the other atom type (Na or Cs). Therefore, we have developed C-S-H and C-A-S-H systems in whose nanopores Ca, Cs, Na, with a Cs/Na ratio of 1, compete for the available sorption sites on the surface.

As we did before, we have analyzed the distribution of the cations in

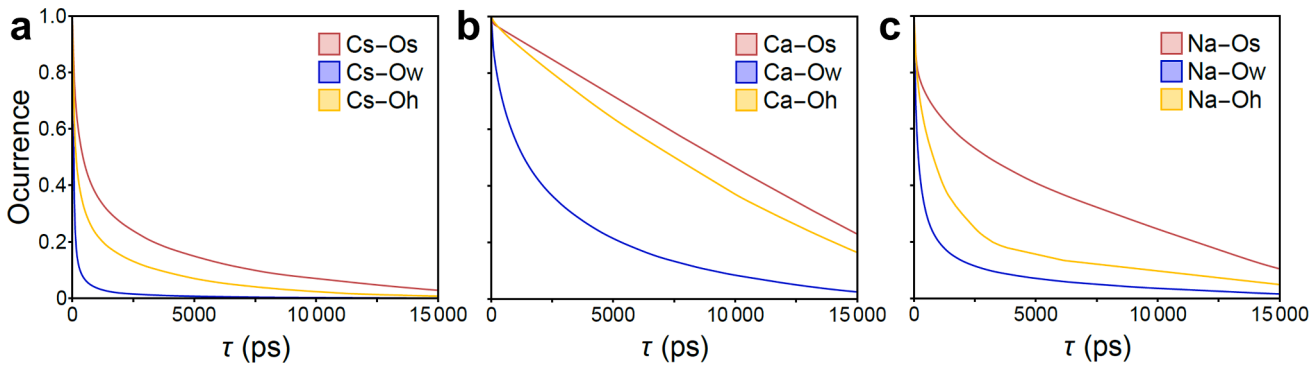

Fig. 4. Autocorrelation functions of (a) Cs-O, (b) Ca-O and (c) Na-O. Cation-surface (M−Os) is shown in garnet, cation-water molecules (M−Ow) in blue and cation-hydroxyl groups (M−Oh) in yellow.

the C-(A-)S-H nanopores by computing the atomic density profile, shown in Fig. 5. Similar to the density profiles of the previously studied systems, Ca can be located below and above the upper interfacial limit, indicating that Ca forms both inner- and outer-sphere complexes. However, there is a remarkable difference between Cs and Na: the peaks assigned to the former cation correspond to outer-sphere complexes, while Na can be found mainly as inner-sphere complexes.

Fig. 5 also shows that the main difference in the cation distribution in C-S-H and C-A-S-H is the proportion of desorbed Cs in the pore space, considerably bigger in the former and negligible in the latter. The relative amounts of Cs, Na and Ca in each sorption configuration are shown in Table 7. The better retention of Na and Ca can be justified by the more negative adsorption enthalpies (see Table 5) that results in more favorable adsorption in the available sorption sites than for Cs ions. Likewise, the more favorable adsorption enthalpies in C-A-S-H due to the Al (see Table 5) incorporation results in better retention concerning C-S-H.

Table 7
Percentage of ions adsorbed in inner-sphere/outer-sphere/pore configurations for the studied cations in C-S-H (left) and C-A-S-H (right).

	C-S-H			C-A-S-H		
Cation	Inner	Outer	Pore	Inner	Outer	Pore
Cs	11%	43%	46%	5%	71%	24%
Ca	44%	56%	0%	55%	45%	0%
Na	51%	38%	11%	61%	33%	6%

The data shown in Table 7 evidence that Cs cations cannot displace

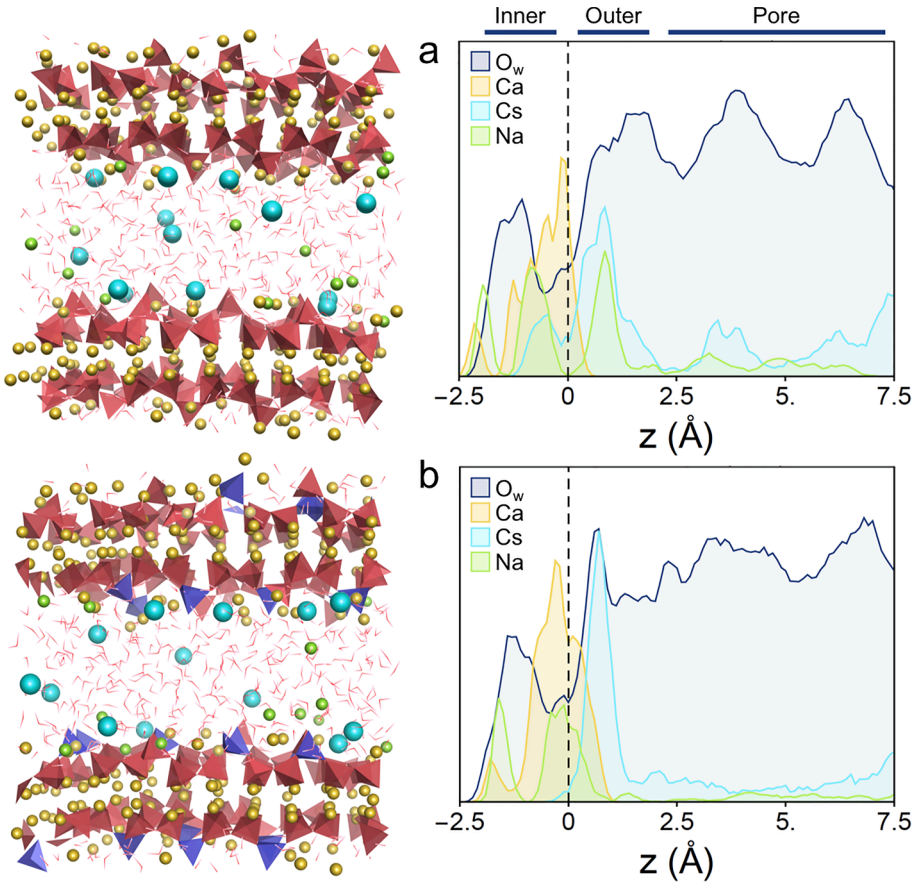

Fig. 5. Density profiles (right) and their corresponding snapshots (left) of the MD simulation for (a) C-S-H and (b) C-A-S-H which incorporate Cs (light blue), Ca (yellow) and Na (purple). The color code is the same as Fig. 2.

Na or Ca cations from the high-affinity sites of the C-(A-)S-H surface. Therefore, the presence of other alkali and alkaline earth cations worsens the Cs uptake both in C-S-H and C-A-S-H. This is due to the low charge density of Cs in comparison with Na and Ca, resulting in lower electrostatic interactions between Cs ions and the C-(A-)S-H surfaces.

As mentioned before, the sorption configuration influences the diffusivity of the adsorbed cations, in such a way that the better the cations are retained the lower their diffusion coefficients. Thus, it can be seen in Table 8 that the lowest diffusion coefficients correspond to Na ions followed by Ca cations. On the other hand, the higher amount of Cs desorbed and in the outer-sphere configuration is reflected in much higher average diffusion coefficients.

3.8. Pore size effect

The size, distribution, connectivity and water content of the pores play a key role in the diffusion of the confined ions in calcium silicate hydrates. Calcium silicate hydrates are layered structures that form a solid network with pores widths from less than 1 nm to above 100 nm, where evaporable water can also be present depending on the relative humidity [85–87]. In this study, we have focused on 1 nm pores, but to study the effect of the pore size in the adsorption and diffusion of the confined cations in gel pores, we have expanded gradually the pore space from 1 nm to 5 nm, distance from which it is considered to reach bulk water behavior. The C-A-S-H model analyzed in the previous section, direct competition, is taken for this study, expanding its pore space from 1 nm to 5 nm gradually. We have expanded the pore up to 5 nm since, at that distance, water located in the center of the pore recovers the diffusivity of bulk water, as explained below. Thereby, from 5 nm, water behaves as bulk water and, consequently, the transport properties of the cations confined in larger pores will be similar. The expanded pores are filled with water molecules up to reach a density of 1 g/cm^3, while the amounts of Cs, Na and Ca are not altered.

First, we have analyzed the arrangement of the confined species in the C-A-S-H pore spaces with different sizes by computing the atomic density profiles, as shown in Fig. 6. It must be noted that only the proximities to the C-A-S-H surface (up to 7.5 Å) are shown to compare and better visualize the adsorption of the cations in this region.

It can be seen in Fig. 6 that most of the cations remain close to the C-A-S-H surfaces, both below and above the upper interfacial limit (z = 0 Å), forming inner- and outer-sphere complexes, notwithstanding there are differences depending on the cation type. All Ca ions are adsorbed on the C-A-S-H surface and no desorbed Ca ions are found at any pore size. Likewise, Na ions tend to remain close to the C-A-S-H surface, but there are small populations of Na in the center of the pore, indicating that a small fraction of Na can be desorbed as discussed below. Finally, most of the Cs ions are located in the proximities of the C-A-S-H surface, although at further distances than Na and Ca ions due to their much higher size. However, there is a significant population of desorbed Cs ions in the pore space at any pore size. To analyze better the sorption configuration of the confined cations, we have estimated the relative amount of Cs, Na and Ca in each sorption configuration for all the analyzed pore sizes (see Table 9).

From these data, it can be drawn that the sorption configuration of the cations is affected by the pore size but it does not change drastically as the pore is expanded since the C-A-S-H surface is the same in all the systems and, consequently, their high affinity sites are not altered. Thus, Cs are mainly forming outer-sphere complexes, while Na and Ca ions are more likely to be as inner-sphere complexes, which is related to the charge density of the analyzed cations, as discussed before. Nevertheless, it is observed that as the pore is expanded, the amount of Cs adsorbed in outer-sphere sorption sites decreases, while the amount of non-adsorbed Cs increases. This rise in the amount of non-adsorbed Cs can be attributed to the higher water content and larger distances to the C-A-S-H surfaces for the cations located in the center of the pore, which facilitates the solvation of the Cs ions by water molecules into stable configurations. The amount of Ca forming inner-sphere complexes increases gradually with the pore expansion, which results in a reduction of the number of outer-sphere complexes. The strong electrostatic interactions between the Ca ions (with divalent charge) and the C-A-S-H surface explain the fact that no desorption is observed at any pore size. Finally, the trend is not clear for non-adsorbed Na cations, although it can be seen that inner-sphere complexation is favored as the pore is expanded regarding outer-sphere complexation.

We have also studied the effect of the pore size on the diffusivity of water molecules, Cs and Na ions. Fig. 7 shows the evolution of the diffusion coefficients as a function of the distance to the C-A-S-H surface for water, Cs and Na ions. Ca is not analyzed since all Ca ions are adsorbed on the surface and the diffusivity does not vary significantly as the pore is expanded.

The evolution of the water diffusivity shown in Fig. 7a does not reveal significant differences in the water diffusivity at the different pore sizes in the proximities of the surface, but in the center of the pore these differences became very pronounced. This is due to the fading of the nanoconfinement effect as the pore space is expanded, resulting in higher water diffusivities up to reach that of bulk water. Indeed, in the center of the pore of 5 nm, the bulk water diffusivity is reached, with values of about $2.4{\cdot}10^{-9}$ m^2/s, in the line with the experimental ($2.3{\cdot}10^{-9}$ m^2/s)[79] and simulated ($2.5{\cdot}10^{-9}$ m^2/s)[80] values measured for bulk water. Therefore, the bulk water behavior is recovered in the center of pores with widths larger than 5 nm.

Likewise, the diffusivity of Cs and Na is also affected by the pore size, as shown in Fig. 7b and 7c. As for water molecules, in the proximities of the C-A-S-H gel, the diffusivity of Cs and Na does not change significantly with the pore sizes. In inner-sphere sorption configurations, Cs ions exhibit average diffusion coefficients of about $2.76{\cdot}10^{-12}$ m^2/s and about $5.06{\cdot}10^{-12}$ m^2/s in outer-sphere sorption sites, while for Na these average coefficients are slightly smaller, about $0.81{\cdot}10^{-12}$ m^2/s and $3.61{\cdot}10^{-12}$ m^2/s, respectively. By contrast, non-adsorbed cations experience considerably higher diffusivities as the pore increases. In fact, for Cs ions, the diffusivity in the largest pore (5 nm) is one order of magnitude higher than in the 1 nm pore, going from about $0.35{\cdot}10^{-9}$ m^2/s (at 1 nm) to $1.95{\cdot}10^{-9}$ m^2/s (at 5 nm), following the trend of water diffusivity. In this way, the diffusivity of Cs ions approximates to that of Cs in bulk water in the center of the pore of 5 nm ($2.1{\cdot}10^{-9}$ m^2/s [73]). Regarding Na diffusivity, it must be noted that there are desorbed Na ions in the pore, but it is scarcer than Cs and it does not reach the center of the pore, in which water diffusivity is maximum, so the estimation of the diffusion coefficients of Na ions along the pore is limited and the maximum diffusivity measured (about $0.78{\cdot}10^{-9}$ m^2/s in the 5 nm pore) is far from its value in bulk water ($1.33{\cdot}10^{-9}$ m^2/s [73]).

Table 8
Average diffusion coefficients for Cs, Na and Ca confined in C-S-H (above) and C-A-S-H (below).

D_{ave} (10^{-12} m^2/s)	C-S-H	C-A-S-H
Cs	59.831	27.886
Ca	0.593	0.179
Na	4.094	3.923

4. Conclusions

In this work, we have studied the retention and diffusivity of Cs, Ca and Na in C-S-H and C-A-S-H, exploring the competition of these ions for the available sorption sites and the effect of aluminum incorporation. For that purpose, we have built C-S-H and C-A-S-H models with a Ca/Si ratio of 1.1 and an Al/Si ratio of 0.15 for C-A-S-H. We have introduced Cs, Ca and Na at a constant concentration of 1.62 cations per nm^2 of C-(A-)S-H surface in nanopores of 1 nm. In this way, we were able to evaluate the affinity and competition of the cations under study for the sorption sites, as well as study their diffusion behavior and the impact of

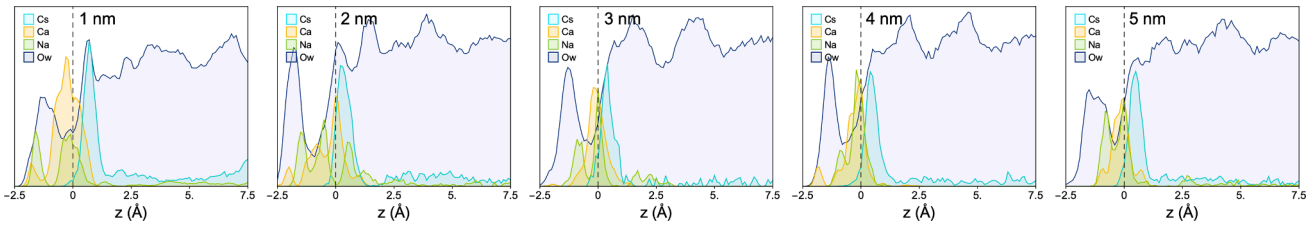

Fig. 6. Density profiles of the confined species in the pores of C-A-S-H expanded from 1 nm (left) to 5 nm (right). The color code is the same as in Fig. 2 and 5.

Table 9
Percentage of ions adsorbed in inner-sphere/outer-sphere/pore configurations for the analyzed pore sizes.

	Cs			Ca			Na		
Cation	Inner	Outer	Pore	Inner	Outer	Pore	Inner	Outer	Pore
1 nm	5%	71%	24%	55%	45%	0%	61%	33%	6%
2 nm	8%	65%	27%	53%	47%	0%	60%	29%	11%
3 nm	7%	73%	20%	58%	42%	0%	67%	26%	7%
4 nm	5%	67%	28%	61%	39%	0%	73%	26%	1%
5 nm	8%	62%	30%	64%	34%	0%	64%	25%	10%

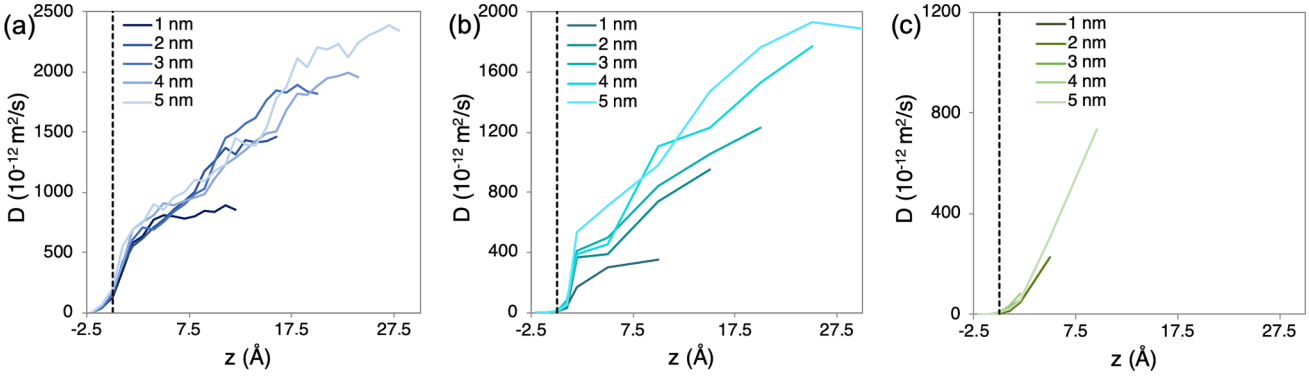

Fig. 7. Average diffusion coefficient of (a) water molecules, (b) Cs and (c) Na ions as a function of the distance from the C-A-S-H surface for the analyzed pore sizes.

aluminum incorporation to form C-A-S-H.

We have seen notable differences between the studied cations; high adsorption and low diffusivity for Na and Ca ions against poor retention of Cs and diffusion coefficients up to two orders of magnitude higher in comparison. These differences between cations may be attributed to their size and charge. The higher the charge density, the stronger the electrostatic interactions with the surface. The size also plays a key role, the high size of the cations and their solvation shells can make difficult the approach to the sorption sites of C-(A-)S-H surfaces. Likewise, Ca and Na ions exhibit high adsorption enthalpies and residence times in high-affinity sites, while the residence time of Cs ions is very small in comparison and its adsorption, although is favorable, is not as much as for Ca and Na. It is also remarkable the great impact on the diffusivity of the aluminum incorporation, particularly significant for Cs, whose diffusion coefficient is reduced up to 40% in C-A-S-H regarding C-S-H, due to the increase of the electrostatic interactions for the aliovalent substitution of Si for Al. Nevertheless, these substitutions do not alter the composition of the solvation shell of the cations, suggesting that they tend to fill their stable coordination shell independently of the environment.

Therefore, the presence of aluminum in the C-S-H structure enhances the retention of the confined cations in the nanopore, reducing their mobility. Indeed, the number of sorption sites increases for all the cations in C-A-S-H with respect to C-S-H, being up to 18% higher for Cs, moving from 1.1 to 1.3 sites/nm^2. It is remarkable that the effect of the aluminum content is more pronounced for those cations with higher charge density, such as Na and Ca, but even if Cs ions are not as well retained as Ca and Na ones, there is a drastic reduction of the diffusivity of Cs concerning these cations in bulk water and inserted in clay minerals. This is due to the combination of the effect of nanoconfinement, which also reduces notably the water diffusivity and the interaction of the cations with the high-affinity sites of C-(A-)S-H surfaces.

The study of the direct competition of the cations understudy has revealed that Cs cations are not capable of displacing Na and Ca from inner-sphere sorption sites, which results in lower retention and higher diffusion coefficients of Cs cations. Finally, the study of the effect of the pore size in the alkali and alkaline earth cations' uptake shows that retention is not significantly modified, but the diffusion of the non-adsorbed cations increases notably as the pore space is expanded as a consequence of the higher water diffusivity due to the fading of the nanoconfinement effect. Thereby, the release of the confined species by leaching mechanisms are favored in gel pores with larger sizes.

5. Data availability statement

The authors declare that all the data for the construction of the C-S-H models and for supporting the findings of this study are available within the paper and its supplementary information files.

CRediT authorship contribution statement

Eduardo Duque-Redondo: Formal analysis, Investigation, Writing - original draft. **Kazuo Yamada:** Conceptualization, Writing - review & editing, Project administration. **Jorge S. Dolado:** Conceptualization, Writing - review & editing, Supervision. **Hegoi Manzano:**

Conceptualization, Writing - review & editing, Supervision.

Declaration of Competing Interest

The authors declare that they have no known competing financial interests or personal relationships that could have appeared to influence the work reported in this paper.

Acknowledgments

This work was supported by "Departamento de Educación, Política Lingüística y Cultura del Gobierno Vasco" (IT912-16) and the ELKARTEK program. E.D.-R. acknowledges the DIPC and DOKBERRI postdoctoral fellowships. The authors thank for technical and human support provided by IZO-SGI SGIker of UPV/EHU and European funding (ERDF and ESF), as well as the i2basque computing resources. Part of this work was financially supported by the Japan Society for the Promotion of Science (JSPS, No. 17H03292).

Appendix A. Supplementary data

The Supplementary Material contains a detailed description of the coordination shell of the cations under study, as well as the characterization of the sorption configuration of the intrinsic Ca in each system. The diffusivity of the Cs, Na and Ca decomposed for each sorption configuration is also included in the Supplementary Material. Supplementary data to this article can be found online at https://doi.org/10.1016/j.commatsci.2021.110312.

References

[1] J.D. Palmer, G.A. Fairhall, Properties of cement systems containing intermediate level wastes, Cem. Concr. Res. 22 (2–3) (1992) 325–330.
[2] T.M. Krishnamoorthy, S.N. Joshi, G.R. Doshi, R.N. Nair, Desorption kinetics of radionuclides fixed in cement matrix, Nucl. Technol. 104 (1993) 351–357, https://doi.org/10.13182/NT93-A34896.
[3] W.E. Lee, M.I. Ojovan, C.M. Jantzen, Radioactive waste management and contaminated site clean-up: Processes, technologies and international experience, Elsevier, 2013.
[4] C.C.D. Coumes, S. Courtois, Cementation of a low-level radioactive waste of complex chemistry: Investigation of the combined action of borate, chloride, sulfate and phosphate on cement hydration using response surface methodology, Cem. Concr. Res. 33 (2003) 305–316.
[5] W. Kluger, W. Hild, R. Köster, G. Meier, H. Krause, Bituminization of radioactive waste concentrates from reprocessing, nuclear research establishments and nuclear power plants, Kernforschungszentrum Karlsruhe GmbH (Germany) (1980).
[6] W.E. Lee, M.I. Ojovan, M.C. Stennett, N.C. Hyatt, Immobilisation of radioactive waste in glasses, glass composite materials and ceramics, Adv. Appl. Ceram. 105 (1) (2006) 3–12.
[7] A.S. Barinov, M.I. Ozhovan, I.A. Sobolev, N.V. Ozhovan, Potential hazard of solidified radioactive wastes, Radiokhimiya 32 (1990) 127–131.
[8] K.G. Papadokostaki, A. Savidou, Study of leaching mechanisms of caesium ions incorporated in Ordinary Portland cement, J. Hazard. Mater. 171 (1–3) (2009) 1024–1031, https://doi.org/10.1016/j.jhazmat.2009.06.118.
[9] K. Volchek, M.Y. Miah, W. Kuang, Z. DeMaleki, F.H. Tezel, Adsorption of cesium on cement mortar from aqueous solutions, J. Hazard. Mater. 194 (2011) 331–337, https://doi.org/10.1016/j.jhazmat.2011.07.111.
[10] F. Macášek, Sorption and leaching properties of the composites and complexes of natural microporous materials, Nat. Microporous Mater. Environ. Technol. (1999) 109–135, https://doi.org/10.1007/978-94-011-4499-5_8. Springer.
[11] J. Real, F. Persin, C. Camarasa-Claret, Mechanisms of desorption of 134 Cs and 85 Sr aerosols deposited on urban surfaces, J. Environ. Radioact. 62 (1) (2002) 1–15, https://doi.org/10.1016/S0265-931X(01)00136-9.
[12] M.I. Ojovan, W.E. Lee, An introduction to nuclear waste immobilisation, Elsevier, 2013.
[13] O.P. Shrivastava, T. Verma, P.K. Wattal, Intrinsic sorption potential of aluminum-substituted calcium silicate hydroxy hydrate for cesium-137, Adv. Cem. Based Mater. 2 (2) (1995) 80–83.
[14] F.P. Glasser, M. Atkins, Cements in radioactive waste disposal, MRS Bull. 19 (1994) 33–38, https://doi.org/10.1557/S0883769400048673.
[15] N.D.M. Evans, Binding mechanisms of radionuclides to cement, Cem. Concr. Res. 38 (4) (2008) 543–553, https://doi.org/10.1016/j.cemconres.2007.11.004.
[16] M. Ochs, D. Mallants, L. Wang, in: Radionuclide and Metal Sorption on Cement and Concrete, Springer International Publishing, 2015, https://doi.org/10.1007/978-3-319-23651-3.
[17] S. Bagosi, L.J. Csetényi, Caesium immobilisation in hydrated calcium-silicate-aluminate systems, Cem. Concr. Res. 28 (12) (1998) 1753–1759, https://doi.org/10.1016/S0008-8846(98)00163-X.
[18] R.O. Abdel Rahman, D.H.A. Zin El Abidin, H. Abou-Shady, Cesium binding and leaching from single and binary contaminant cement–bentonite matrices, Chem. Eng. J. 245 (2014) 276–287.
[19] C. Shi, A. Fernández-Jiménez, Stabilization/solidification of hazardous and radioactive wastes with alkali-activated cements, J. Hazard. Mater. 137 (3) (2006) 1656–1663, https://doi.org/10.1016/j.jhazmat.2006.05.008.
[20] M. Tsuji, S. Komarneni, P. Malla, Substituted tobermorites: 27Al and 29Si MAS NMR, cation exchange, and water sorption studies, J. Am. Ceram. Soc. 74 (2) (1991) 274–279, https://doi.org/10.1111/jace:1991.74.issue-210.1111/j.1151-2916.1991.tb06874.x.
[21] S. Komarneni, R. Roy, D.M. Roy, C.A. Fyfe, G.J. Kennedy, A.A. Bothner-By, J. Dadok, A.S. Chesnick, 27Al and 29Si magic angle spinning nuclear magnetic resonance spectroscopy of Al-substituted tobermorites, J. Mater. Sci. 20 (11) (1985) 4209–4214.
[22] S. Komarneni, D.M. Roy, C.A. Fyfe, G.J. Kennedy, Naturally occurring 1.4 nm tobermorite and synthetic jennite: characterization by 27Al and 29Si MASNMR spectroscopy and cation exchange properties, Cem. Concr. Res. 17 (6) (1987) 891–895, https://doi.org/10.1016/0008-8846(87)90077-9.
[23] S. Komarneni, M. Tsuji, Selective cation exchange in substituted tobermorite, J. Am. Ceram. Soc. 72 (1989) 1668–1674, https://doi.org/10.1111/j.1151-2916.1989.tb06301.x.
[24] M. Miyake, S. Komarneni, R. Roy, Kinetics, equilibria and thermodynamics of ion exchange in substituted tobermorites, Mater. Res. Bull. 24 (3) (1989) 311–320, https://doi.org/10.1016/0025-5408(89)90217-1.
[25] S. Komarneni, D.M. Roy, New tobermorite cation exchangers, J. Mater. Sci. 20 (8) (1985) 2930–2936, https://doi.org/10.1007/BF00553057.
[26] M. Tsuji, S. Komarneni, Alkali metal ion exchange selectivity of Al-substituted tobermorite, J. Mater. Res. 4 (3) (1989) 698–703.
[27] A.G. Kalinichev, R.J. Kirkpatrick, Molecular dynamics modeling of chloride binding to the surfaces of calcium hydroxide, hydrated calcium aluminate, and calcium silicate phases, Chem. Mater. 14 (8) (2002) 3539–3549, https://doi.org/10.1021/cm0107070.
[28] HARRY.F.W. TAYLOR, Proposed structure for calcium silicate hydrate gel, J. Am. Ceram. Soc. 69 (6) (1986) 464–467, https://doi.org/10.1111/jace:1986.69.issue-610.1111/j.1151-2916.1986.tb07446.x.
[29] I.G. Richardson, The nature of the hydration products in hardened cement pastes, Cem. Concr. Compos. 22 (2) (2000) 97–113, https://doi.org/10.1016/S0958-9465(99)00036-0.
[30] L.B. Skinner, S.R. Chae, C.J. Benmore, H.R. Wenk, P.J.M. Monteiro, Nanostructure of calcium silicate hydrates in cements, Phys. Rev. Lett. 104 (2010) 195502_1–195502_4, https://doi.org/10.1103/PhysRevLett.104.195502.
[31] S.-Y. Hong, F.P. Glasser, Alkali sorption by CSH and CASH gels: Part II. Role of alumina, Cem. Concr. Res. 32 (7) (2002) 1101–1111.
[32] J. Yang, Y. Jia, D. Hou, P. Wang, Z. Jin, H. Shang, S. Li, T. Zhao, Na and Cl immobilization by size controlled calcium silicate hydrate nanometer pores, Constr. Build. Mater. 202 (2019) 622–635.
[33] N. Loganathan, A.O. Yazaydin, G.M. Bowers, A.G. Kalinichev, R.J. Kirkpatrick, Structure, energetics, and dynamics of Cs+ and H2O in hectorite: Molecular dynamics simulations with an unconstrained substrate surface, J. Phys. Chem. C. 120 (2016) 10298–10310.
[34] J. Jiang, P. Wang, D. Hou, The mechanism of cesium ions immobilization in the nanometer channel of calcium silicate hydrate: A molecular dynamics study, Phys. Chem. Chem. Phys. 19 (41) (2017) 27974–27986, https://doi.org/10.1039/C7CP05437H.
[35] J. Bu, R. Gonzalez Teresa, K.G. Brown, F. Sanchez, Adsorption mechanisms of cesium at calcium-silicate-hydrate surfaces using molecular dynamics simulations, J. Nucl. Mater. 515 (2019) 35–51.
[36] E. Duque-Redondo, Y. Kazuo, I. López-Arbeloa, H. Manzano, Cs-137 immobilization in C-S-H gel nanopores, Phys. Chem. Chem. Phys. 20 (14) (2018) 9289–9297, https://doi.org/10.1039/C8CP00654G.
[37] E. Duque-Redondo, K. Yamada, H. Manzano, Cs retention and diffusion in C-S-H at different Ca/Si ratio, Cem. Concr. Res. 140 (2021) 106294, https://doi.org/10.1016/j.cemconres.2020.106294.
[38] J. Arayro, A. Dufresne, T. Zhou, K. Ioannidou, J.-F. Ulm, R. Pellenq, L.K. Béland, Thermodynamics, kinetics, and mechanics of cesium sorption in cement paste: A multiscale assessment, Phys. Rev. Mater. 2 (2018) 53608.
[39] G. Kovačević, B. Persson, L. Nicoleau, A. Nonat, V. Veryazov, Atomistic modeling of crystal structure of Ca1.67SiHx, Cem. Concr. Res. 67 (2015) 197–203.
[40] F.P. Glasser, Characterisation of the barrier performance of cements, in: MRS Proc., Cambridge Univ Press, 2002: pp. 721–732. https://doi.org/10.1557/PROC-713-JJ9.1.
[41] S.-Y. Hong, F.P. Glasser, Alkali binding in cement pastes: Part I. The CSH phase, Cem. Concr. Res. 29 (12) (1999) 1893–1903, https://doi.org/10.1016/S0008-8846(99)00187-8.
[42] E. Bonaccorsi, S. Merlino, A.R. Kampf, The crystal structure of tobermorite 14 A (Plombierite), a C-S-H phase, J. Am. Ceram. Soc. 88 (3) (2005) 505–512, https://doi.org/10.1111/jace:2005.88.issue-3.
[43] I.G. Richardson, The calcium silicate hydrates, Cem. Concr. Res. 38 (2) (2008) 137–158, https://doi.org/10.1016/j.cemconres.2007.11.005.
[44] I.G. Richardson, Tobermorite/jennite- and tobermorite/calcium hydroxide-based models for the structure of C-S-H: applicability to hardened pastes of tricalcium silicate, beta-dicalcium silicate, Portland cement, and blends of Portland cement

with blast-fumace slag, metaka, Cem. Concr. Res. 34 (2004) 1733–1777, https://doi.org/10.1016/j.cemconres.2004.05.034.
[45] J.M. Martínez, L. Martínez, Packing optimization for automated generation of complex system's initial configurations for molecular dynamics and docking, J. Comput. Chem. 24 (2003) 819–825, https://doi.org/10.1002/jcc.10216.
[46] L. Martínez, R. Andrade, E.G. Birgin, J.M. Martínez, PACKMOL: A package for building initial configurations for molecular dynamics simulations, Wiley Subscription Services, Inc., A Wiley Company, 2009. https://doi.org/10.1002/jcc.21224.
[47] X. Pardal, F. Brunet, T. Charpentier, I. Pochard, A. Nonat, 27Al and 29Si solid-state NMR characterization of calcium-aluminosilicate-hydrate, Inorg. Chem. 51 (3) (2012) 1827–1836.
[48] F. Puertas, M. Palacios, H. Manzano, J.S. Dolado, A. Rico, J. Rodríguez, A model for the CASH gel formed in alkali-activated slag cements, J. Eur. Ceram. Soc. 31 (12) (2011) 2043–2056.
[49] K. Chenoweth, A.C.T. van Duin, W.A. Goddard, ReaxFF reactive force field for molecular dynamics simulations of hydrocarbon oxidation, J. Phys. Chem. A. 112 (5) (2008) 1040–1053, https://doi.org/10.1021/jp709896w.
[50] J.C. Fogarty, H.M. Aktulga, A.Y. Grama, A.C.T. van Duin, S.A. Pandit, A reactive molecular dynamics simulation of the silica-water interface, J. Chem. Phys. 132 (2010) 174704_1–174704_10, https://doi.org/10.1063/1.3407433.
[51] K.L. Joshi, A.C.T. van Duin, Molecular dynamics study on the Influence of additives on the high-temperature structural and acidic properties of ZSM-5 zeolite, Energy Fuels. 27 (8) (2013) 4481–4488.
[52] H. Manzano, R.J.M. Pellenq, F.-J. Ulm, M.J. Buehler, A.C.T. van Duin, Hydration of calcium oxide surface predicted by reactive force field molecular dynamics, Langmuir 28 (9) (2012) 4187–4197, https://doi.org/10.1021/la204338m.
[53] M.B. Pinson, E. Masoero, P.A. Bonnaud, H. Manzano, Q. Ji, S. Yip, J.J. Thomas, M. Z. Bazant, K.J. Van Vliet, H.M. Jennings, Hysteresis from multiscale porosity: Modeling water sorption and shrinkage in cement paste, Phys. Rev. Appl. 3 (2015) 64009_1–64009_17.
[54] R. Shahsavari, R.-M. Pellenq, F.-J. Ulm, Empirical force fields for complex hydrated calcio-silicate layered materials, Phys. Chem. Chem. Phys. 13 (3) (2011) 1002–1011, https://doi.org/10.1039/C0CP00516A.
[55] R.T. Cygan, J.-J. Liang, A.G. Kalinichev, Molecular models of hydroxide, oxyhydroxide, and clay phases and the development of a general force field, J. Phys. Chem. B. 108 (4) (2004) 1255–1266, https://doi.org/10.1021/jp0363287.
[56] J. Åqvist, Ion-water interaction potentials derived from free energy perturbation simulations, J. Phys. Chem. 94 (21) (1990) 8021–8024, https://doi.org/10.1021/j100384a009.
[57] S. Plimpton, Fast parallel algorithms for short-range molecular dynamics, J. Comput. Phys. 117 (1) (1995) 1–19, https://doi.org/10.1006/jcph.1995.1039.
[58] P.P. Ewald, Die Berechnung optischer und elektrostatischer Gitterpotentiale, Ann. Phys. 369 (3) (1921) 253–287, https://doi.org/10.1002/(ISSN)1521-388910.1002/andp.v369:310.1002/andp.19213690304.
[59] L. Verlet, Computer" experiments" on classical fluids. I. Thermodynamical properties of Lennard-Jones molecules, Phys. Rev. 159 (1) (1967) 98–103, https://doi.org/10.1103/PhysRev.159.98.
[60] J.J. Chen, J.J. Thomas, H.F.W. Taylor, H.M. Jennings, Solubility and structure of calcium silicate hydrate, Cem. Concr. Res. 34 (9) (2004) 1499–1519, https://doi.org/10.1016/j.cemconres.2004.04.034.
[61] M.J. Abdolhosseini Qomi, K.J. Krakowiak, M. Bauchy, K.L. Stewart, R. Shahsavari, D. Jagannathan, D.B. Brommer, A. Baronnet, M.J. Buehler, S. Yip, F.-J. Ulm, K. J. Van Vliet, R.J.M. Pellenq, Combinatorial molecular optimization of cement hydrates, Nat. Commun. 5 (2014) 1–10, https://doi.org/10.1038/ncomms5960.
[62] X. Cong, R.J. Kirkpatrick, 29Si MAS NMR study of the structure of calcium silicate hydrate, Adv. Cem. Based Mater. 3 (3-4) (1996) 144–156, https://doi.org/10.1016/S1065-7355(96)90046-2.
[63] J.S. Dolado, M. Griebel, J. Hamaekers, A molecular dynamic study of cementitious calcium silicate hydrate (C–S–H) gels, J. Am. Ceram. Soc. 90 (2007) 3938–3942, https://doi.org/10.1111/j.1551-2916.2007.01984.x.
[64] J.J. Thomas, J.J. Chen, H.M. Jennings, D.A. Neumann, Ca-OH bonding in the C-S-H gel phase of tricalcium silicate and white portland cement pastes measured by inelastic neutron scattering, Chem. Mater. 15 (20) (2003) 3813–3817, https://doi.org/10.1021/cm034227f.
[65] E.A. Guggenheim Thermodynamics-an advanced treatment for chemists and physicists, 1985.
[66] T.E. Payne, V. Brendler, M. Ochs, B. Baeyens, P.L. Brown, J.A. Davis, C. Ekberg, D. A. Kulik, J. Lutzenkirchen, T. Missana, Y. Tachi, L.R. Van Loon, S. Altmann, Guidelines for thermodynamic sorption modelling in the context of radioactive waste disposal, Environ. Model. Softw. 42 (2013) 143–156.
[67] I. Androniuk, C. Landesman, P. Henocq, A.G. Kalinichev, Adsorption of gluconate and uranyl on CSH phases: Combination of wet chemistry experiments and molecular dynamics simulations for the binary systems, Phys. Chem. Earth Parts A/B/C. 99 (2017) 194–203.
[68] I.C. Bourg, G. Sposito, Molecular dynamics simulations of the electrical double layer on smectite surfaces contacting concentrated mixed electrolyte (NaCl–CaCl2) solutions, J. Colloid Interface Sci. 360 (2011) 701–715, https://doi.org/10.1016/j.jcis.2011.04.063.
[69] M. Brehm, B. Kirchner, TRAVIS – A free analyzer and visualizer for Monte Carlo and molecular dynamics trajectories, J. Chem. Inf. Model. 51 (8) (2011) 2007–2023, https://doi.org/10.1021/ci200217w.
[70] A. Einstein, Über die von der molekularkinetischen Theorie der Wärme geforderte Bewegung von in ruhenden Flüssigkeiten suspendierten Teilchen, Ann. Phys. 322 (8) (1905) 549–560, https://doi.org/10.1002/(ISSN)1521-388910.1002/andp.v322:810.1002/andp.19053220806.
[71] J.C. Slater, Atomic radii in crystals, J. Chem. Phys. 41 (10) (1964) 3199–3204, https://doi.org/10.1063/1.1725697.
[72] R.D.t. Shannon, Revised effective ionic radii and systematic studies of interatomic distances in halides and chalcogenides, Acta Crystallogr. Sect. A Cryst. Physics, Diffraction, Theor. Gen. Crystallogr. 32 (1976) 751–767.
[73] Li Yuan-Hui, Sandra Gregory, Diffusion of ions in sea water and in deep-sea sediments, Geochim. Cosmochim. Acta. 38 (5) (1974) 703–714, https://doi.org/10.1016/0016-7037(74)90145-8.
[74] R. Mills, Self-diffusion in normal and heavy water in the range 1–45.deg, J. Phys. Chem. 77 (5) (1973) 685–688, https://doi.org/10.1021/j100624a025.
[75] Andrey G. Kalinichev, Jianwei Wang, R. James Kirkpatrick, Molecular dynamics modeling of the structure, dynamics and energetics of mineral-water interfaces: Application to cement materials, Cem. Concr. Res. 37 (3) (2007) 337–347, https://doi.org/10.1016/j.cemconres.2006.07.004.
[76] Hegoi Manzano, Sina Moeini, Francis Marinelli, Adri C.T. van Duin, Franz-Josef Ulm, Roland J.-M. Pellenq, Confined water dissociation in microporous defective silicates: mechanism, dipole distribution, and impact on substrate properties, J. Am. Chem. Soc. 134 (4) (2012) 2208–2215, https://doi.org/10.1021/ja209152n.
[77] Mohammad Javad Abdolhosseini Qomi, Mathieu Bauchy, Franz-Josef Ulm, Roland J.-M. Pellenq, Anomalous composition-dependent dynamics of nanoconfined water in the interlayer of disordered calcium-silicates, J. Chem. Phys. 140 (5) (2014) 054515, https://doi.org/10.1063/1.4864118.
[78] Patrick A. Bonnaud, Hegoi Manzano, Ryuji Miura, Ai Suzuki, Naoto Miyamoto, Nozomu Hatakeyama, Akira Miyamoto, Temperature dependence of nanoconfined water properties: application to cementitious materials, J. Phys. Chem. C. 120 (21) (2016) 11465–11480, https://doi.org/10.1021/acs.jpcc.6b0094410.1021/acs.jpcc.6b00944.s001.
[79] K. Krynicki, C.D. Green, D.W. Sawyer, Pressure and temperature dependence of self-diffusion in water, Faraday Discuss. Chem. Soc. 66 (1978) 199–208, https://doi.org/10.1039/DC9786600199.
[80] M.W. Mahoney, W.L. Jorgensen, Diffusion constant of the TIP5P model of liquid water, J. Chem. Phys. 114 (2001) 363–366, https://doi.org/10.1063/1.1329346.
[81] V. Marry, P. Turq, Microscopic simulations of interlayer structure and dynamics in bihydrated heteroionic montmorillonites, J. Phys. Chem. B. 107 (8) (2003) 1832–1839.
[82] Fang-Ru Chou Chang, N.T. Skipper, Garrison Sposito, Monte Carlo and molecular dynamics simulations of interfacial structure in lithium-montmorillonite hydrates, Langmuir 13 (7) (1997) 2074–2082.
[83] C.A.J. Appelo, L.R. Van Loon, P. Wersin, Multicomponent diffusion of a suite of tracers (HTO, Cl, Br, I, Na, Sr, Cs) in a single sample of Opalinus Clay, Geochim. Cosmochim. Acta. 74 (4) (2010) 1201–1219.
[84] J.J. Tuck, P.L. Hall, M.H.B. Hayes, D.K. Ross, C. Poinsignon, Quasi-elastic neutron-scattering studies of the dynamics of intercalated molecules in charge-deficient layer silicates. Part. 1.—Temperature dependence of the scattering from water in Ca 2+-exchanged montmorillonite, J. Chem. Soc. Faraday Trans. 1 Phys. Chem. Condens. Phases. 80 (1984) 309–324.
[85] N. Malikova, V. Marry, J.-F. Dufrêche, P. Turq, Na/Cs montmorillonite: temperature activation of diffusion by simulation, Curr. Opin. Colloid Interface Sci. 9 (1–2) (2004) 124–127.
[86] Tamotsu Kozaki, Hiroki Sato, Seichi Sato, Hiroshi Ohashi, Diffusion mechanism of cesium ions in compacted montmorillonite, Eng. Geol. 54 (1–2) (1999) 223–230.
[87] Haruo Sato, Takashi Ashida, Yukitoshi Kohara, Mikazu Yui, Noriaki Sasaki, Effect of dry density on diffusion of some radionuclides in compacted sodium bentonite, J. Nucl. Sci. Technol. 29 (9) (1992) 873–882.
[88] Fang-Ru Chou Chang, N.T. Skipper, Garrison Sposito, Computer simulation of interlayer molecular structure in sodium montmorillonite hydrates, Langmuir 11 (7) (1995) 2734–2741.